14. J. Weissmüller, *J. Non-Cryst. Solids* **142**, 70 (1992).
15. D. B. Miracle, *Nat. Mater.* **3**, 697 (2004).
16. H. W. Sheng *et al.*, *Nature* **439**, 419 (2006).
17. Our unpublished measurements on the liquid eutectic alloys of AuSn and AuGe yielded layering peaks 30 to 50 times lower than that of AuSi.
18. O. G. Shpyrko *et al.*, *Phys. Rev. Lett.* **95**, 106103 (2005).
19. Details of the GIXD experiment are available on *Science* Online.
20. Because of insufficient reproducibility, the discussion of this pattern must be deferred.
21. S. K. Sinha, E. B. Sirota, S. Garoff, H. B. Stanley, *Phys. Rev. B* **38**, 2297 (1988).
22. A. K. Green, E. Bauer, *J. Appl. Phys.* **47**, 1284 (1976).
23. J. F. Chang *et al.*, *Mat. Chem. Phys.* **83**, 199 (2004).
24. H. S. Chen, D. Turnbull, *J. Appl. Phys.* **38**, 3646 (1967).
25. S. L. Molodtsov, C. Laubschat, G. Kaindl, A. M. Shikin, V. K. Adamchuk, *Phys. Rev. B* **44**, 8850 (1991).
26. V. A. Filonenko, *Russ. J. Phys. Chem.* **43**, 874 (1969).
27. L. Bischoff, J. Teichert, T. Ganetsos, G. L. R. Mair, *J. Phys. D Appl. Phys.* **33**, 692 (2000).
28. J. B. Hannon, S. Kodambaka, F. M. Ross, R. M. Tromp, *Nature* **440**, 69 (2006).
29. Y. T. Cheng, L. W. Lin, K. Najafi, *J. Microelectromech. Syst.* **9**, 3 (2000).

30. This work was supported by the U.S. Department of Energy (DOE) grant DE-FG02-88-ER45379 and the U.S.-Israel Binational Science Foundation, Jerusalem. Brookhaven National Laboratory is supported by U.S. DOE contract DE-AC02-98CH10886. We acknowledge beamline assistance from J. Gebhardt, T. Graber, and H. Brewer at the Chemistry and Materials Science Sector of the Center for Advanced Radiation Sources (ChemMatCARS). ChemMatCARS Sector 15 is principally supported by NSF/DOE grant CHE0087817. The Advanced Photon Source is supported by U.S. DOE contract W-31-109-Eng-38.

Supporting Online Material
www.sciencemag.org/cgi/content/full/313/5783/77/DC1
Materials and Methods
Fig. S1
References and Notes

4 April 2006; accepted 25 May 2006
10.1126/science.1128314

Probing the Solvent-Assisted Nucleation Pathway in Chemical Self-Assembly

Pascal Jonkheijm,[1]* Paul van der Schoot,[2] Albertus P. H. J. Schenning,[1]† E. W. Meijer[1]†

Hierarchical self-assembly offers a powerful strategy for producing molecular nanostructures. Although widely used, the mechanistic details of self-assembly processes are poorly understood. We spectroscopically monitored a nucleation process in the self-assembly of π-conjugated molecules into helical supramolecular fibrillar structures. The data support a nucleation-growth pathway that gives rise to a remarkably high degree of cooperativity. Furthermore, we characterize a helical transition in the nucleating species before growth. The self-assembly process depends strongly on solvent structure, suggesting that an organized shell of solvent molecules plays an explicit role in rigidifying the aggregates and guiding them toward further assembly into bundles and/or gels.

Chemical self-assembly offers a very attractive approach for constructing complex, supramolecular nanostructures. Hierarchical processes, typical of chemical self-assembly, spontaneously produce ordered ensembles of single or multiple molecular components and are ubiquitous in chemistry, physics, materials science, and biology (*1*). For example, a large variety of molecules has been reported that form gels through three-dimensional networks of (bundles of) fibers (*2*). Highly versatile biomaterials have been produced by self-assembly of peptide amphiphiles (*3*), and (semi)conducting tubes and rods have been achieved from properly chosen π-conjugated oligomeric building blocks (*4*). In many cases, the resulting fibrillar structures are helical, and a preferred handedness is obtained by the introduction of stereocenters into the building blocks (*5*). Ensuring that the components aggregate in a specific motif, however, remains a formidable task; molecular components are easily trapped in kinetically stable arrangements of varying topology (*6*). The application of spectroscopy in combination with scattering and microscopy techniques has provided a reasonable view of the final self-assembled structures, yet a thorough understanding of the processes leading up to these structures remains elusive. Unravelling such structural pathways is crucial for the widely sought goal of extending rational synthesis into the nanoscale regime (*7*).

Although the growth of fibrillar structures typically requires nucleation, prior studies have not focused on the nature and properties of the nuclei. This lack of data is in sharp contrast to the abundant studies on the crystallization of small molecules (*8*) or polymers (*9*), and on the aggregation of proteins (*10*). For instance, notable insight into the formation of actin filaments, microtubules, and viral capsids by a nucleation-growth mechanism was obtained after the pioneering work of Klug (*11*) and Caspar (*12*). More recently, this insight was used to study pathologies stemming from amyloid deposits and diseases related to protein aggregation (*13*). Phenomenologically, the different phases of protein aggregation should be very similar to those involved in chemical self-assembly. Two models are commonly invoked to describe protein aggregation. Isodesmic self-assembly (*10*), also called multistage open association or ladder- or free-association model, is noncooperative, and the association constant is independent of the size of the object. Nucleated self-assembly, also called nucleation growth or initiation elongation, is characterized by a size-dependent association constant that gives rise to cooperative kinetics. We have sought to characterize such processes in chemical synthetic systems.

The fibrillar structures we examined comprise oligo(*p*-phenylenevinylene) derivatives (OPV-*x*) with chiral side chains capped on one end by a tridodecyloxybenzene and on the other by a ureidotriazine tailored for self-complementary fourfold hydrogen bonding (structure shown in Fig. 1) (*14*, *15*). Previous

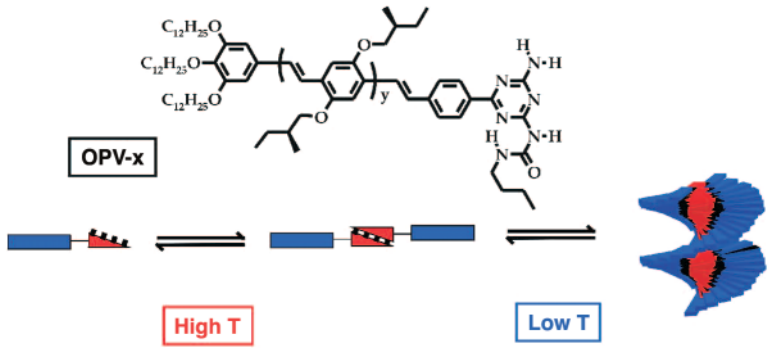

Fig. 1. Molecular structure of the oligo(*p*-phenylenevinylene) derivatives OPV-*x* [for OPV-3, *y* (number of dialkoxybenzene units) = 1; OPV-4, *y* = 2; and OPV-5, *y* = 3] and schematic representation of the self-assembly process, with blue blocks representing the OPV backbone and red wedges representing the hydrogen-bonding end groups.

[1]Laboratory of Macromolecular and Organic Chemistry, [2]Polymer Physics Group, Eindhoven University of Technology, Post Office Box 513, 5600 MB Eindhoven, Netherlands.

*Present address: Chemical Biology, Max Planck Institute for Molecular Physiology, Otto Hahnstrasse 11, 44227 Dortmund, Germany.

†To whom correspondence should be addressed. E-mail: e.w.meijer@tue.nl (E.W.M.); a.p.h.j.schenning@tue.nl (A.P.H.J.S.)

temperature-dependent ultraviolet and visible absorption (UV/vis), fluorescence, and circular dichroism (CD) measurements (fig. S1) (*14*, *15*) revealed two different states of the π-conjugated chromophores in dodecane solution: discrete monomeric or hydrogen-bonded dimeric species at high temperature and helical aggregates at low temperature (Fig. 1). The hydrogen-bonded dimers have been studied in detail with scanning tunneling microscopy (STM) (*16*) and ^{1}H nuclear magnetic resonance (NMR) spectroscopy (*14*), whereas the fibrillar structural dimensions have been measured by small angle neutron scattering (SANS) and atomic force microscopy (AFM) (*15*). For example, OPV-4 exhibited a fibril persistence length of 150 nm and diameter of 5.8 nm in dodecane (table S1). The diameters of the fibrils were in close agreement with molecular modeling studies (table S1). Fluorescence microscopy revealed a perpendicular chromophore orientation within the fibrils (*17*).

By improving our spectroscopic sensitivity, we reveal in this study distinct hierarchical stages that govern the formation process of helical OPV-4 aggregates. Optical probing is a powerful technique on account of the extreme sensitivity of the π-conjugated chromophore to conformational, orientational, and supramolecular states of the OPV compound. We have analyzed the data with a model similar to the Oosawa-Kasai model for helical assembly of proteins in solution (*18*–*21*), which yields thermodynamic information such as the mean size of the assemblies as well as the equilibrium constants. Moreover, we uncovered the explicit role of the solvent molecules in the formation of the supramolecular stacks. Our findings can be generally applied to many chemical self-assembly processes of ordered quasi-one-dimensional stacks.

By using CD spectroscopy at a specific wavelength, we could monitor the optical changes characterizing the crossover from the monomeric state of OPV-4 to the aggregated state in dodecane. A Peltier-temperature programmer for thermostatting the samples was used to cool the solution slowly in small steps (from 375 K to 275 K, with a rate of 0.5 K/min and a resolution of one data point per 0.1 K). The slow cooling is necessary to suppress kinetic (i.e., nonequilibrium) effects on the self-assembly (fig. S2, A and B). We tracked the growth in the intensity of the λ = 466 nm CD band for four different OPV-4 concentrations and consistently observed a sharp increase at a specific temperature (fig. S2C), indicative of the transition from monomers into helical aggregates with a preferred handedness. This curve is not sigmoidal, and hence it cannot be described by an isodesmic model. However, it does follow expected Oosawa-Kasai behavior

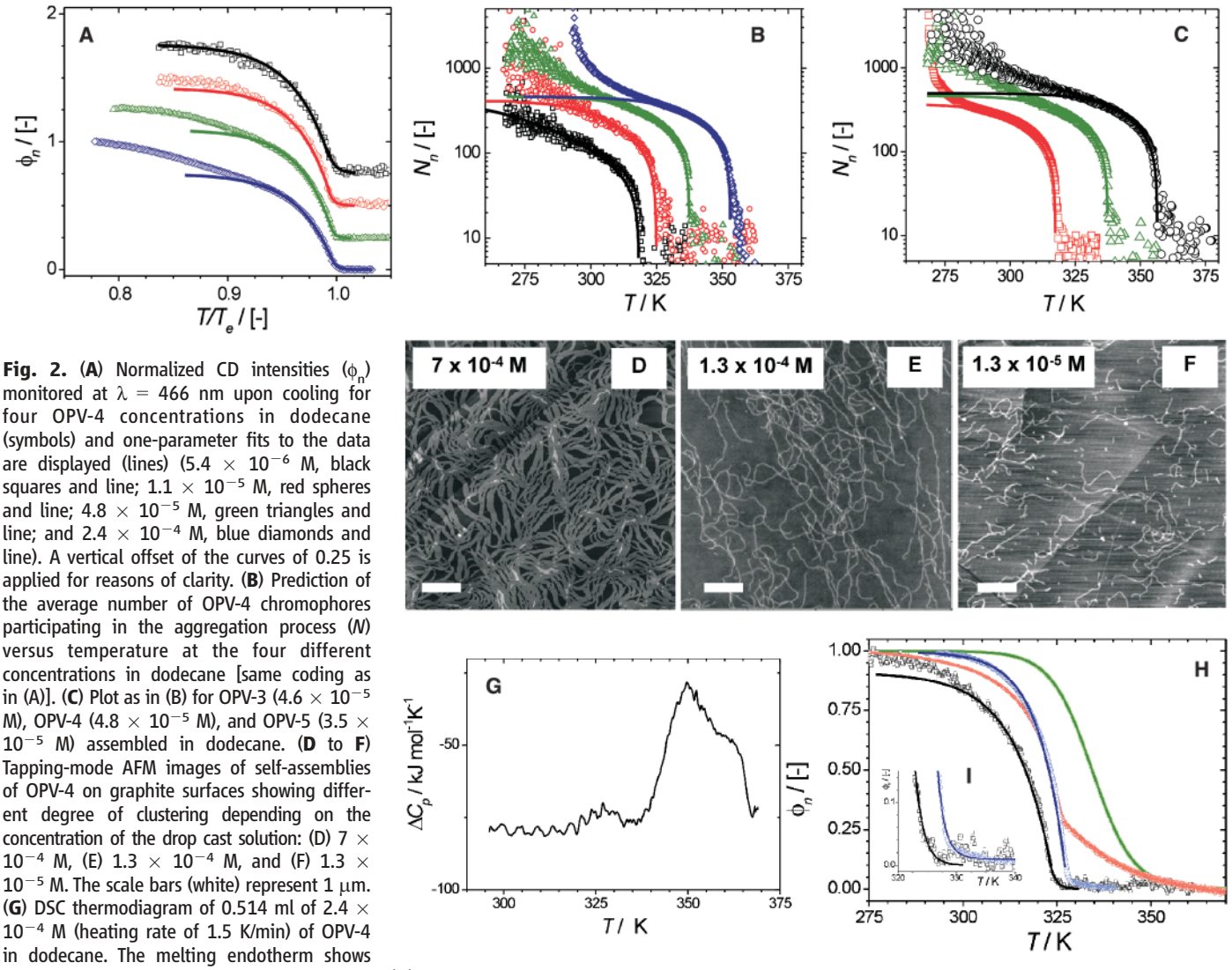

Fig. 2. (**A**) Normalized CD intensities (ϕ_n) monitored at λ = 466 nm upon cooling for four OPV-4 concentrations in dodecane (symbols) and one-parameter fits to the data are displayed (lines) (5.4×10^{-6} M, black squares and line; 1.1×10^{-5} M, red spheres and line; 4.8×10^{-5} M, green triangles and line; and 2.4×10^{-4} M, blue diamonds and line). A vertical offset of the curves of 0.25 is applied for reasons of clarity. (**B**) Prediction of the average number of OPV-4 chromophores participating in the aggregation process (*N*) versus temperature at the four different concentrations in dodecane [same coding as in (A)]. (**C**) Plot as in (B) for OPV-3 (4.6×10^{-5} M), OPV-4 (4.8×10^{-5} M), and OPV-5 (3.5×10^{-5} M) assembled in dodecane. (**D** to **F**) Tapping-mode AFM images of self-assemblies of OPV-4 on graphite surfaces showing different degree of clustering depending on the concentration of the drop cast solution: (D) 7×10^{-4} M, (E) 1.3×10^{-4} M, and (F) 1.3×10^{-5} M. The scale bars (white) represent 1 μm. (**G**) DSC thermodiagram of 0.514 ml of 2.4×10^{-4} M (heating rate of 1.5 K/min) of OPV-4 in dodecane. The melting endotherm shows transition temperatures at 351.0 K and 361.7 K. (**H**) Transition curves based on UV/vis [λ = 490 nm (green) and λ = 335 nm (blue)], fluorescence (λ = 500 nm), and CD (λ = 466 nm) spectra for OPV-4 (1.1×10^{-5} M). Fits to the data are shown on the basis of isodesmic or cooperative self-assembly. (**I**) A closer view of the nucleation regime based on the UV-vis (λ = 335 nm) and CD data.

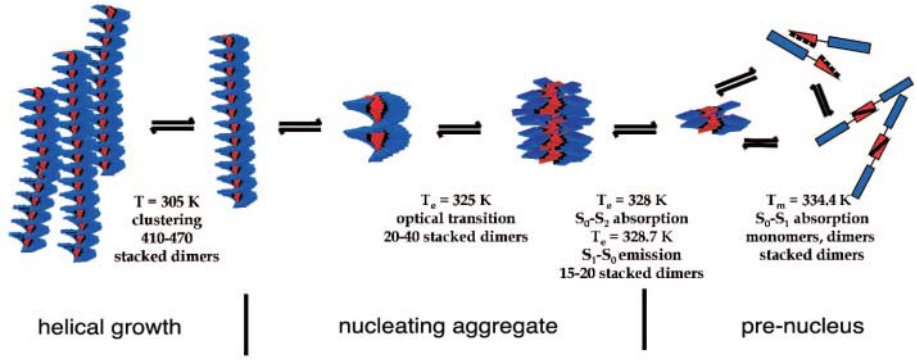

Fig. 3. Schematic representation of the hierarchical self-assembly of OPV-4 in solution based on the measurements presented in Fig. 2. First, monomers form dimers via quadruple hydrogen bonding. Upon cooling, about 10 to 15 dimers are brought together via an isodesmic pathway, forming disordered stacks. Upon further cooling, the molecules in the preaggregates become more restricted in relative position via a cooperative process (T_e = 328 K). In the next step, the preaggregates undergo a coil-helix transition to form a chiral nucleus of about 28 dimers, at which point the elongation-growth pathway sets in. Lastly, the cooperative stack length is reached and clustering of the assemblies occurs.

for thermally activated equilibrium polymerization (*19*), in which the non-isodesmic helical assembly (characterized by an activation step and subsequent propagation steps) is preceded by the isodesmic assembly of nonhelical structures. The modified model is a mathematically more tractable version of a self-assembled Ising chain theory introduced to describe the helix-coil transition in supramolecular polymers (*22*, *23*). In the simplified model, the two kinds of assemblies are linked through equilibrium between nonhelical and helical assemblies of a critical size (*19*). According to the model, the number average aggregation number of the helical assemblies N obeys the following relationship:

$$K_e = \exp[h_e(T - T_e)/RT_e^2] = 1 - N^{-1} + K_a N(N - 1) \quad (1)$$

with K_e as the equilibrium constant of the elongation process, K_a the equilibrium constant of the activation step, T the absolute temperature, h_e the molecular enthalpy of the elongation process, and R the gas constant. The fraction of molecules in assemblies, ϕ_n, obeys approximately

$$\{1 - \exp[h_e(T - T_e)/RT_e^2]\} \quad (2)$$

in the helical polymerized regime $T < T_e$ and approximates

$$\{K_a^{1/3}\exp[(2/3K_a^{-1/3} - 1)h_e(T - T_e)/RT_e^2]\} \quad (3)$$

near the polymerization temperature T_e [Supporting Online Material (SOM) Text]. Applying this model to our data, we can estimate N, the mean number of dimers in the aggregate, from Eq. 1; T_e, the temperature at which elongation sets in, ϕ_n, the normalized fraction of molecules in the aggregate, and h_e, the enthalpy of bond formation from both Eqs. 2 and 3; and K_a, the equilibrium constant between the active and nonactive state, from Eq. 3; active meaning the state that can initiate the elongation.

The normalized CD curves (Fig. 2A) are well fit by Eqs. 2 and 3, showing unambiguously that our model description is internally consistent and that helical aggregates are not present above the characteristic T_e (i.e., for values of T/T_e in excess of unity) but form only after the sharp nucleation step. The T_e decreases upon diluting the sample, revealing a linear relationship in the Van't Hoff plot (fig. S2D), with $\Delta H = -100$ kJ/mol and $\Delta S = -215$ J/mol K. Although there is a good correlation between experiment and theory in the case of the most dilute solution (5.4 μM) (Fig. 2A), at higher concentrations the theory underestimates the CD data at low temperatures (i.e., low T/T_e) (Fig. 2A). This result suggests an additional process that is not considered in the current polymerization theory. Interestingly, the fits for the different concentrations show that the temperature at which theory deviates from experiment (T_{sat}) rises with increasing concentration. This deviation is also visible in a plot of N versus temperature (Fig. 2B). At lower temperatures, the average columnar length estimated from the fitted model is remarkably constant for N values from 410 to 470. Assuming a π-π stacking distance of 0.35 nm (*15*), this N range corresponds to a length of 145 to 165 nm. These values are comparable with the values found by SANS and AFM [150 and 125 nm, respectively (table S1)]. With these data in hand, the deviation from one-dimensional growth at higher concentrations can be attributed as the clustering of stacks (both laterally and along the growing direction, Fig. 2, D to F). The data suggest this clustering is isodesmic in nature (fig. S3).

At the helical polymerization temperature $T = T_e$, the theory allows for the calculation of K_a: We find values of 2.0×10^{-4}, 0.46×10^{-4}, 0.31×10^{-4}, and 0.15×10^{-4}, in order from lowest to highest starting OPV concentra-

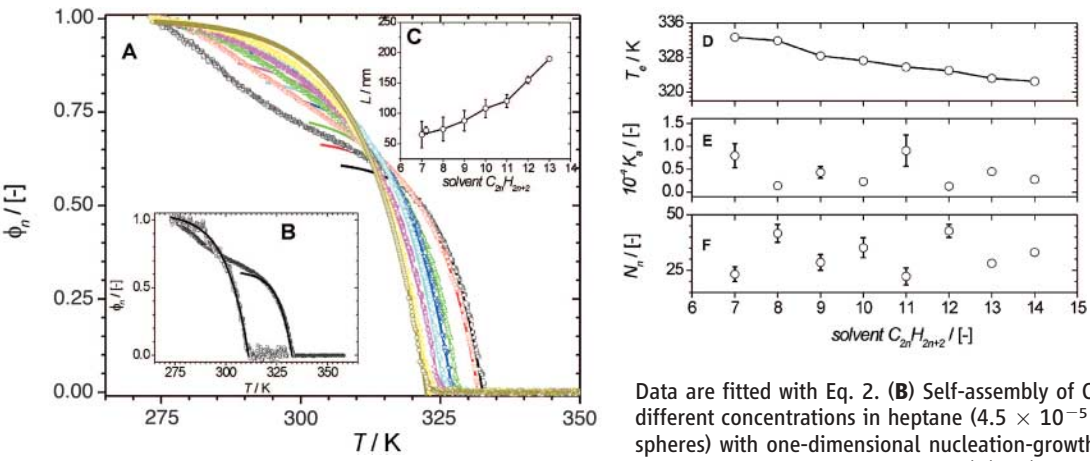

Fig. 4. Solvent-dependent CD measurements of OPV-4 in eight alkane solvents. (**A**) The normalized aggregate fraction of self-assembled OPV-4 in alkane solvents versus T/T_e [4.5×10^{-5} M $C_{2n}H_{2n+2}$, where n values were 7 (black), 8 (red), 9 (green), 10 (blue), 11 (cyan), 12 (magenta), 13 (yellow), and 14 (dark yellow)] based on monitoring CD intensity at λ = 466 nm upon cooling. Data are fitted with Eq. 2. (**B**) Self-assembly of OPV-4 versus temperature at two different concentrations in heptane (4.5×10^{-5} M, squares, and 4.5×10^{-6} M, spheres) with one-dimensional nucleation-growth fits. (**C**) Cooperative length (L) for OPV-4 in the different solvents, (**D**) T_e (accuracy is 0.1 K based on the fit), (**E**) K_a (error based on the determination of ϕ_{sat}), and (**F**) N are plotted versus number of carbons in alkane solvent (fig. S9). Error bars are based on the fit.

tion (Fig. 2A). The transition from the nonhelical state to the helical preaggregates is a prerequisite for spontaneous growth of the helix at temperatures below T_e (below $T/T_e = 1$) (fig. S2C); this behavior underlies the cooperative effect. From the plot in fig. S2E it is possible to estimate the average size of preaggregates or nuclei at $T = T_e$. The size of these nuclei, given by $N \sim K_a^{-1/3}$, thus yields chiral nuclei of 17 to 41 hydrogen-bonded dimers in order of ascending concentration at T_e. Computer simulations of the photophysical properties of the stacks suggested rotation angles between adjacent stacked dimers in the range of 6° to 12° (*24*). Intriguingly, in order to complete one helical pitch (180°), 15 to 30 stacked hydrogen-bonded dimers are needed. The rapid growth from these helical nuclei is caused by the many reinforcing noncovalent interactions and is enthalpy-driven, with an excess bond formation enthalpy of h_e = –56 kJ/mol estimated from the slope at T_e. The stability of the preaggregates is expected to increase when additional π-π interactions are provided by extending the chromophore length. Consistent with this reasoning, we observed that the T_e shifts from 317.5 K for OPV-3 to 325.0 K for OPV-4 and then to 356.5 K for OPV-5 (Fig. 2C) for comparable concentrations. Also, the length of the different molecular stacks can be estimated. The values of circa (ca.) 125 nm for the OPV-3 stack and ca. 175 nm for the OPV-5 stack bracket that of the OPV-4 stack (150 nm) and are in agreement with SANS data (table S1) (*15*).

The strong endotherm measured with ultrasensitive differential scanning calorimetry (DSC) confirms the high cooperativity of the polymerization. The DSC curve (Fig. 2G) shows the presence of two transitions, one broad transition from 340 to 365 K, coinciding with the absorption data (see below), and one sharp transition at 351 K. The latter coincides with the T_e extracted from the CD measurements. At these transition temperatures, we also observe the largest volume changes in preliminary pressure perturbation calorimetric experiments. Further research is needed to correlate the thermodynamic parameters, acquired with the different techniques, to the individual steps in the self-assembly process (Fig. 3). To obtain a more detailed picture of the characteristics of the nuclei, we turned to fluorescence and UV/vis spectroscopy, again using the same slow cooling rate of 0.5 K/min to suppress kinetic (nonequilibrium) effects (Fig. 2H). Careful analysis of the UV/vis and fluorescence data (Fig. 2, H and I, and SOM Text) reveals experimental evidence for both isodesmic (by using eq. S3) and cooperative transitions (by using Eqs. 2 and 3) at different temperatures (figs. S4 to S6).

Combining all data, it is possible to postulate a hierarchical pathway for the self-assembly of OPV-4 into fibrillar structures upon cooling a solution of molecularly dissolved monomers at high temperature (Fig. 3). First, the monomers form dimers via quadruple hydrogen bonding. The association of the very first hydrogen-bonded dimers into short stacks having disorder both inside the molecules as well as in the stacking direction follows an isodesmic pathway. This isodesmic equilibrium state continues to shift upon cooling until 10 to 15 stacked dimers are brought together, characterized by sigmoidal transitions in the UV/vis spectrum [T_m = 334.4 K, absorption at λ = 490 nm, $S_0 \rightarrow S_1$ transition (Fig. 2H)] and fluorescence data (first part of the melting curve in Fig. 2H). Upon further cooling, the molecules in the preaggregates become more restricted in their relative positions, characterized by the abrupt change at T_e = 328 K in the absorption at λ = 335 nm [more localized $S_0 \rightarrow S_2$ transition (*25*) (Fig. 2, H and I)] and in the fluorescence spectra [(Fig. 2H) quenching is presumably related to faster diffusion of excitons to trap sites (*26*) due to improved ordering (fig. S6)]. This cooperative transition is close to the onset of chiroptical activity in the preaggregates (Fig. 2I). Helix formation transforms the preaggregate into a chiral nucleus of 28 dimers (fig. S4) (at a concentration of 1.1×10^{-5} M, $K_a = 0.46 \times 10^{-4}$) before the elongation-growth pathway sets in, as detected by the cooperative CD transition. The persistence length of the structures is independent of concentration but depends on the size of the molecule. Concentration, on the other hand, determines the temperature at which the onset of clustering occurs.

We have found that solvent structure dramatically influences the stability of the nuclei and stacks (Fig. 4). Upon changing the length of the alkane solvent in the self-assembly process (fig. S7), the T_e shifts from 322.5 (tetradecane) to 332.7 K (heptane) as measured at constant chromophore concentration (Fig. 4A). The observed change is not linear but shows an oscillatory dependence on whether the solvent contains an odd or even number of carbons (Fig. 4D). When K_a as well as N is plotted versus the number of C atoms in the solvent, a strong odd-even effect again is observed (Fig. 4, E and F). Nearly all physical parameters in alkane solvents depend linearly on the number of carbons in the alkane chain except for properties related to ordering, such as the density and melting points of the alkanes. It therefore appears that coorganization of the solvent at the periphery of the aggregates plays a direct role in the assembly process, evident even during the formation of the preaggregates. Whereas the full assembly curve measured in tetradecane can be fitted with a one-dimensional growth model, this model underestimates the experimental data measured in other solvents. The point of deviation, however, occurs at different temperatures depending on the length of the solvent molecule. In the shortest solvent chains, the self-assembly is apparently by far the most sensitive for clustering, and the average columnar length is shortest (Fig. 4C and fig. S8). This finding has important consequences for understanding the different properties found for the same molecular stacks formed in different solvents and suggests that the solvent does not play a passive role in supramolecular assembly, but rather must be considered explicitly.

On one hand, our study shows that the expected nucleation-growth mechanism is applicable to chemical self-assembly structures. On the other hand, unexpected details about the nucleating species and persistency and the role of the solvent have become visible. All of these findings are potentially relevant to the formation processes of fibers, gels, and other supramolecular structures in general.

References and Notes

1. G. M. Whitesides, M. Boncheva, *Proc. Natl. Acad. Sci. U.S.A.* **99**, 4769 (2002).
2. P. Terech, R. G. Weiss, *Chem. Rev.* **97**, 3133 (1997).
3. T. Shimizu, M. Masuda, H. Minamikawa, *Chem. Rev.* **105**, 1401 (2005).
4. F. J. M. Hoeben, P. Jonkheijm, E. W. Meijer, A. P. H. J. Schenning, *Chem. Rev.* **105**, 1491 (2005).
5. J. J. L. M. Cornelissen, A. E. Rowan, R. J. M. Nolte, N. A. J. M. Sommerdijk, *Chem. Rev.* **101**, 4039 (2001).
6. A. Lohr, M. Lysetska, F. Würthner, *Angew. Chem. Int. Ed. Engl.* **44**, 5071 (2005).
7. R. F. Service, *Science* **309**, 95 (2005).
8. B. Moulton, M. J. Zaworotko, *Chem. Rev.* **101**, 1629 (2001).
9. P. J. Flory, *J. Chem. Phys.* **17**, 223 (1949).
10. A. Kentsis, K. L. B. Borden, *Curr. Protein Peptide Sci.* **5**, 125 (2004).
11. A. Klug, *Philos. Trans. R. Soc. London Ser. B* **354**, 531 (1999).
12. D. L. Caspar, *Biophys. J.* **32**, 103 (1980).
13. R. Krishnan, S. L. Lindquist, *Nature* **435**, 765 (2005).
14. A. P. H. J. Schenning, P. Jonkheijm, E. Peeters, E. W. Meijer, *J. Am. Chem. Soc.* **123**, 409 (2001).
15. P. Jonkheijm *et al.*, *J. Am. Chem. Soc.* **125**, 15941 (2003).
16. A. Gesquière *et al.*, *Nano Lett.* **4**, 1175 (2004).
17. C. R. L. P. N. Jeukens *et al.*, *J. Am. Chem. Soc.* **127**, 8280 (2005).
18. F. Oosawa, M. Kasai, *J. Mol. Biol.* **4**, 10 (1962).
19. P. van der Schoot, in *Supramolecular Polymers*, A. Ciferri, Ed. (CRC Press, Baton Rouge, LA, 2005).
20. A. Aggeli *et al.*, *Proc. Natl. Acad. Sci. U.S.A.* **98**, 11857 (2001).
21. F. Oosawa, S. Asakura, *Thermodynamics of the Polymerization of Proteins* (Academic Press, London, 1975).
22. J. van Gestel, P. van der Schoot, M. A. J. Michels, *Langmuir* **19**, 1375 (2003).
23. P. van der Schoot, M. A. J. Michels, L. Brunsveld, R. P. Sijbesma, A. Ramzi, *Langmuir* **16**, 10076 (2000).
24. D. Beljonne *et al.*, *J. Phys. Chem. B* **109**, 10594 (2005).
25. L. Herz *et al.*, *Phys. Rev. B* **68**, 045203 (2003).
26. E. Peeters, A. Marcos Ramos, S. C. J. Meskers, R. A. J. Janssen, *J. Chem. Phys.* **112**, 9445 (2000).

27. P.J. was a postdoctoral fellow in the framework of BIOMADE (EU). This work was further financially supported by grants from the Dutch Council for Sciences (NWO). We thank F. J. M. Hoeben for providing the OPV-3; R. A. J. Janssen, L. Brunsveld, M. van Genderen, and M. Smulders for stimulating discussions; and L. Mitra and R. Winter for collaborating and measuring preliminary calorimetric measurements.

Supporting Online Material

www.sciencemag.org/cgi/content/full/313/5783/80/DC1
Materials and Methods
SOM Text
Figs. S1 to S9
Table S1
References

24 March 2006; accepted 22 May 2006
10.1126/science.1127884